Water Resources Management (2023) 37:4363–4383
https://doi.org/10.1007/s11269-023-03561-6

Analysing the Impact of Land Subsidence on the Flooding Risk: Evaluation Through InSAR and Modelling

María I. Navarro-Hernández[1] · Javier Valdes-Abellan[1] · Roberto Tomás[1] · Serena Tessitore[2] · Pablo Ezquerro[3] · Gerardo Herrera[3]

Received: 30 August 2022 / Accepted: 14 July 2023 / Published online: 2 August 2023

Abstract
Floods greatly impact human settlements in flood risk areas, such as floodplains and coastal lowlands, following heavy rainfall. The Alto Guadalentin valley, an orogenic tectonic depression, experiences extreme flash floods and land subsidence due to groundwater withdrawal, rendering it one of Europe's fastest subsiding regions. In this study, we compared two 2D flood event models representing different land subsidence scenarios for 1992 and 2016. To determine the flooded area and water depth variations due to land subsidence, the Hydrologic Engineering Centre River Analysis System 2D (HEC-RAS 2D) model was used to simulate flood inundation by the Alto Guadalentin River and its tributaries. Synthetic aperture radar (SAR) satellite (ERS, ENVISAT, and Cosmo-SkyMED) images were employed, along with the interferometric SAR (InSAR) technique, to calculate the magnitude and spatial distribution of land subsidence. By analysing the accumulated subsidence distributions obtained from InSAR, the original topography of the valley in 1992 and 2016 was reconstructed. These digital surface models (DSMs) were then used to generate 2D hydraulic models, simulating flood scenarios in the unsteady mode. The results demonstrated significant changes in the water surface elevation over the 14-year period, with a 2.04 km2 increase in areas with water depths exceeding 0.7 m. These findings were utilized to create a flood risk map and assess the economic flood risk. The data highlight the crucial role of land subsidence in determining the inundation risk in the Alto Guadalentin valley, providing valuable insights for emergency management and civil protection against future potential flooding events.

Keywords Flood hazard mapping · HEC-RAS · 2D models · InSAR · Land subsidence · Risk evaluation

1 Introduction

Floods are natural phenomena that occur when the rainfall rate exceeds the infiltration capacity of soil, and the subsequently generated runoff exceeds the usual boundaries of river channels occupying parts of the territory (Schumann 2011). They represent the most frequent extreme occurrences worldwide and cause the highest economic losses relative

Extended author information available on the last page of the article

to other natural disasters (Sarchani et al. 2020). In Spain, floods pose major social and economic threats, leading to more than 200 deaths in recent decades (National Weather Service 2019; Pujadas Ferrer 2002). This is mainly due to its arid climate (prolonged droughts alternated with intense rainfall) that increases the occurrence probability of floods (Sempere et al. 1994) and its geomorphological characteristics (Bodoque et al. 2016).

Climate change has led to changes in rainfall patterns and intensity, resulting in increased occurrences of extreme floods. Projections indicate a doubling of extreme flood events in Europe by 2035 (Marchi et al. 2010; Sarchani et al. 2020). Human settlements located along alluvial fans are particularly vulnerable to floods due to urbanization in these areas. Efforts to mitigate the socioeconomic impacts of flash floods have involved the construction of defence infrastructures and the implementation of improved prediction methods (Mihu-Pintilie et al. 2019). Over time, flood impact reduction strategies have evolved, from hydraulic structures to floodplain management and scenario analysis. Flood modelling using advanced software and remote sensing data has significantly improved flood risk management by reducing uncertainties and generating accurate flood maps that consider climate change effects. These flood maps play a crucial role in risk assessment, enabling flood risk analysis, damage assessment, and effective planning for timely response and protection of communities (Şen 2017; Smith 2013; Xu et al. 2023).

Streamflow hydraulic models are widely used for flood event simulation and management, providing hydraulic variables for scenario analysis (Schumann 2011). The 1D model can be used to efficiently simulate channel flows, but this model requires well-defined channels. In the 2D approach, the study area is discretized as a mesh, allowing visualization of the flood extent, water depth, and velocity, but this technique demands significant computational resources (Cerri 2017; Lea et al. 2019). Finally, 3D models consider three flow velocity components, improving the accuracy by addressing the limitations of 1D and 2D models, but they are computationally demanding and less commonly used due to resource and time constraints (Lauchlan Arrowsmith and Zhu 2014).

The precision of input data is crucial for hydraulic modelling and can be enhanced by various remote sensing technologies such as LiDAR and satellite configurations. These advancements improve flood risk assessments by providing high-resolution digital terrain models (DTMs) for flood mapping (Cerri 2017; Refice et al. 2018; Scarpino et al. 2018). The LiDAR offers detailed topographic information with high accuracy and rapid data collection and is particularly valuable in flood-prone regions. The widely used HEC-RAS software enables 1D and 2D hydraulic calculations and benefits from integrating high-density LiDAR-based DTMs to improve the flood parameter accuracy and risk estimation performance (Brunner 2016; Hutanu et al. 2020). Satellite remote sensing, specifically InSAR, is effective for measuring topography and ground deformation, aiding in land subsidence quantification (Ferretti et al. 2007; Herrera-García et al. 2021; Poreh et al. 2021). Integration of remote sensing technology with HEC-RAS modelling can enhance flood risk assessments by improving the flood parameter accuracy, facilitating high-quality flood mapping, and supporting effective flood hazard management.

The Alto Guadalentin valley exhibits one of the highest subsidence rates due to intensive groundwater withdrawal. This subsidence has resulted in cumulative vertical displacements exceeding 1 m in many areas of the floodplain (Bonì et al. 2015; Ezquerro et al. 2020). In contrast, the valley is characterized by nonsignificant riverbed channels despite high-water flow rates that eventually emerge, making it prone to floods. The valley has been affected by very important flood events, with an average revisiting time of 2 years in recent centuries (Castejón Porcel and Romero Díaz 2014). More recently, during the 1973 event, the Nogalte Stream reached a volumetric flow rate of 2,000 m^3/s

after heavy rainfall totalling 300 mm in two hours. Water exceeded the river channel limits, and water collection systems and agriculture elements were destroyed; 1,430 dwellings were damaged, 13 lives were lost in Lorca, and more than 80 lives were lost in Puerto Lumbreras (García-tornel 2016; Ortega-Becerril et al. 2016; Romera-Franco 2008). Four decades later, in 2012, a rainstorm producing 150 mm in 2 h triggered the Nogalte, Béjar, La Torrecilla, Viznaga ravines and Guadalentín River to burst their banks, killing 8 people and generating severe damage to communication infrastructure, agriculture and livestock production, structures and outbuildings (Gil-Meseguer et al. 2012). The two events in 1973 and 2012 were characterized by a similar discharge, but, as shown by Ortega-Becerril et al. (2016), a new flooding pattern due to a sediment load deficit was observed. According to this study, in-channel gravel mining and aquifer overexploitation may be responsible for the increasing river velocity and stream power in the study area.

In this paper, we conducted rainfall–runoff simulations for the Alto Guadalentin valley considering two scenarios, 1992 and 2016, to explain the cumulative subsidence that occurred in the area during this period. A 2D hydraulic model (HEC-RAS) was employed to estimate changes in the flood extent, water depth, velocity, and economic damage. The two scenarios were obtained through the integration of high-resolution LiDAR DSM data (2.5 m) and satellite-based displacement measurements by incorporating cumulative subsidence data obtained through the InSAR technique during the 1992–2009 and 2009–2016 periods. Finally, the hydraulic model outcomes enabled the assessment of flood-related changes and the quantification of economic damage, accounting for the impact of subsidence. In this study, we introduced a novel multidimensional approach to analyse the consequences of the inefficient management of detrital aquifers based on the integration of LiDAR DSM data analysis, hydraulic modelling and satellite-based displacement estimation. In areas where water overexploitation provoked the compaction of unconsolidated alluvial soils with a consequent subsidence phenomenon, this could result in a change in flood hazards. We analysed such complex cause−effect mechanisms to quantify the economic impact of subsidence on flood-related damage.

2 Study Area

The Alto Guadalentin valley (SE Spain) is a tectonic depression surrounded by mountain ranges. It encompasses an area of approximately 250 km^2 with elevations ranging from 300 to 400 m a.s.l. The principal human settlements in the study area are Lorca with 95,515 inhabitants in 2020, Puerto Lumbreras with 15,780 inhabitants in 2020, and Almendricos with 1,720 inhabitants in 2018 (data from the Spanish National Statistical Office, INE). Notably, 35% of the population resides in dispersed dwellings outside the urban areas known as the Lorca field with 9,478 cadastral units (Cerón 1995). The valley is characterized by a semiarid climate with limited rainfall, averaging 150 mm/year (Fernandez et al. 2018). This basin is filled by Quaternary sediments that have evolved into wide alluvial fan systems developed at the western margin due to their higher slopes than those at the eastern basin margin. The hydrographic network has been modified by geomorphological processes and is characterized by the rapid attainment of the maximum water energy under torrential rainfall. The Guadalentin River is the main watercourse, experiencing low flow rates during dry periods and extreme flow rates up to 3,000 m^3/s during intense storms (Cerón 1995). Other streams, such as the Nogalte, Torrecilla, and Béjar ravines, pose flood hazards in the region (Fig. 1). The Alto Guadalentin aquifer, a sedimentary and multilayer

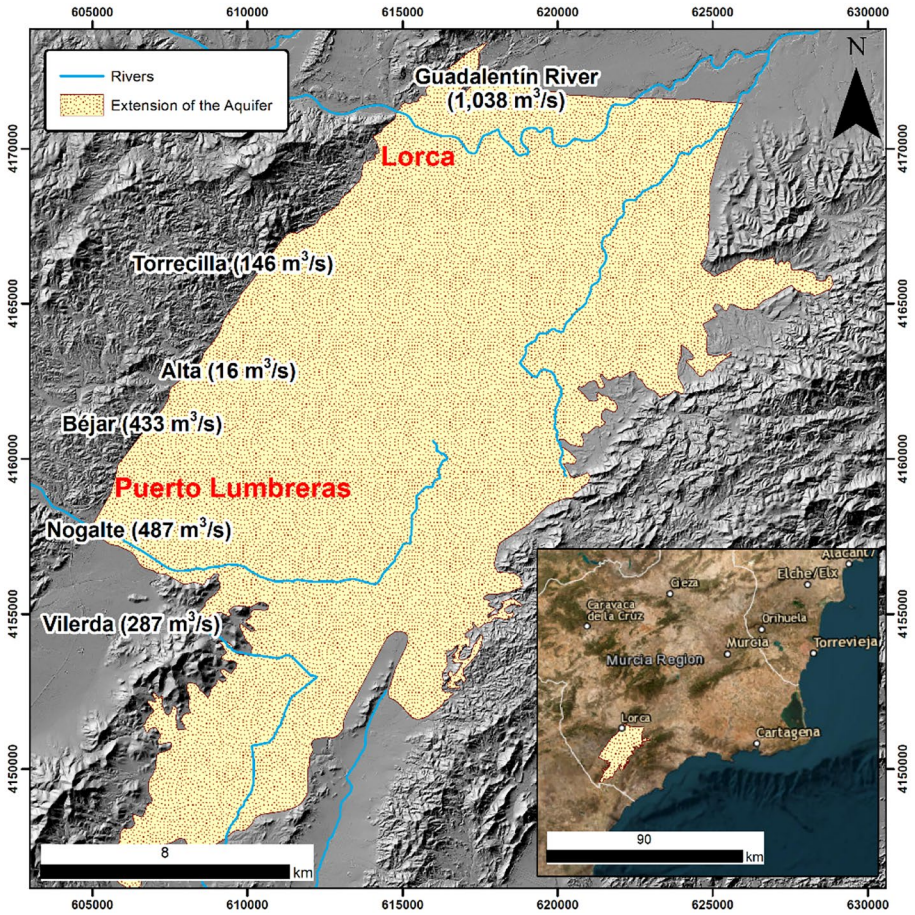

Fig. 1 Location of the study area

system, has been extensively exploited for agricultural purposes since 1960. Excessive groundwater extraction has led to depletion of over 150 m, resulting in the declaration of temporary overexploitation in 1988. While pumping volumes have decreased, soil consolidation continues to cause ground deformation, albeit at a slightly reduced subsidence rate of 10 cm/year versus the initial rate of 13 cm/year (Ezquerro et al. 2020).

3 Data and Methods

In this section, the data and model used to estimate flood hazards in the Alto Guadalentin valley are described. Figure 2 shows a flowchart of the methodology. In Section 3.1, the processing details of the InSAR data used to obtain subsidence maps for the 1992–2016 period are introduced, along with other data utilized as modelling inputs. Section 3.2 provides a detailed account of the model setup. Finally, in Section 3.3, the

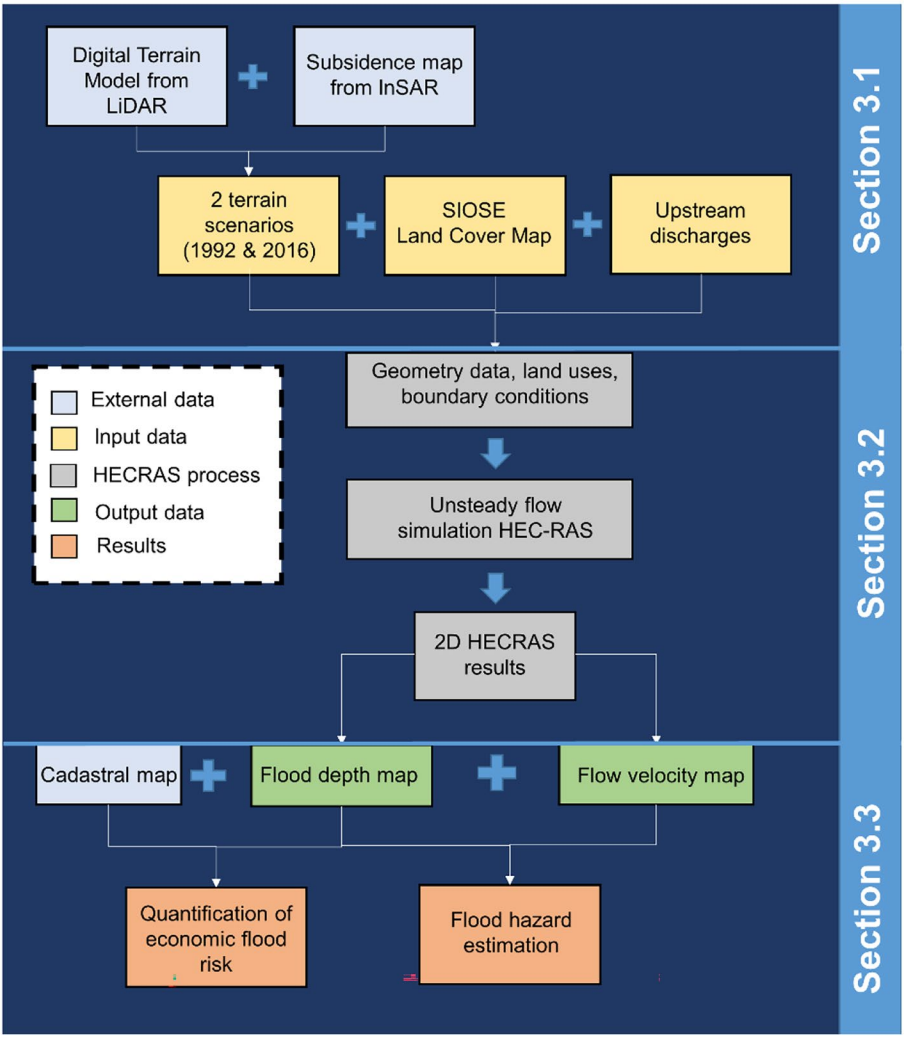

Fig. 2 Flowchart of the applied methodology

hazard index is described, which was adopted to categorize the risk according to the flood depth and velocity.

3.1 Input Data

3.1.1 InSAR data

In the present work, InSAR data obtained from the processing of several SAR datasets through different methods were combined to achieve a cumulative subsidence layer dataset. In the Alto Guadalentín valley, the temporal evolution of deformation from 1992 to 2016 was studied using SAR images retrieved from C- and X-band satellites; specifically, ERS (1992–2000),

ENVISAT (2003–2010) and Cosmo-SkyMED (2011–2016) datasets were used to obtain cumulative displacements for the two considered scenarios (1992 and 2016). Regarding the gap in the monitoring period between ERS and ENVISAT, the mean velocity obtained from ERS data was used to estimate the deformation occurring from 2000–2003. Subsidence values after 2009 include ENVISAT values from 2009 to 2010, CSK measurements (2011–2016) and estimated values from 2010 to 2011 corresponding to ENVISAT data (Bonì et al. 2015; Ezquerro et al. 2020). InSAR displacement data were interpolated using the IDW method (Bartier and Keller 1996) to avoid problems related to the measurement scatterer (MS) density and location between the different processing approaches. Figure 3 shows the cumulative land subsidence after the integration of all InSAR data for the 1992–2016 period, reaching a maximum settlement value up to 2.7 m along the line of sight (LOS) of the satellite.

3.1.2 Land Use and Discharge

A land cover map is provided by the IGN as a dataset model called the SIOSE, which supplies information on the various land uses with a scale of 1:25,000 corresponding to the 2014 version. As shown in Fig. 4, the land cover distribution mainly corresponds to the various agricultural uses within the valley, while residential use is concentrated near the mountainous areas. From the land use information, unique Manning's roughness coefficients were assigned according to Spanish legal instructions for flood mapping of each land cover class (Ministerio de Medio Ambiente, y Medio Rural y Marino 2011).

The 2D boundary condition lines, the principal upstream considered in the simulation and their respective maximum flow rates are shown in Fig. 3. These maximum water flow values correspond to a 100-year return period, and they are supported by previous inundation risk studies led by the Hydrographic Confederation of the Segura River (CHS) (CHS 2014). The downstream boundary condition used for the HEC-RAS model is the normal depth option for the four outflows shown in Fig. 4. Table S1 summarizes all the datasets and information used for flood modelling and flood risk analysis in the Alto Guadalentin valley.

3.1.3 DMS (1992 & 2016)

The digital surface model (DSM) was derived with a resolution of 2.5 m from an aerial LiDAR dataset acquired in 2009 provided by the National Centre for Geographic Information (IGN) of Spain featuring a density of 0.5 dots/m^2. To obtain the two surface scenarios for 1992 and 2016 (shown in Fig. 2), the 2009 DSM was combined with InSAR-measured ground surface changes. Therefore, DSMs were obtained for the 1992 and 2016 scenarios by adding the cumulative land subsidence registered in the study area during the 1992–2009 and 2009–2016 periods. Notably, even though aquifer overexploitation began in the 1960s, the cumulative subsidence considered in the present study starts in 1992, when regular InSAR observations of ground displacements started.

3.2 Model Setup

3.2.1 HEC-RAS 6.0

HEC-RAS software can be employed to simulate different river analysis components for the generation of steady-flow water surface profiles, unsteady flow simulations, sediment transport computations and water quality analysis. For 2D unsteady flow, the

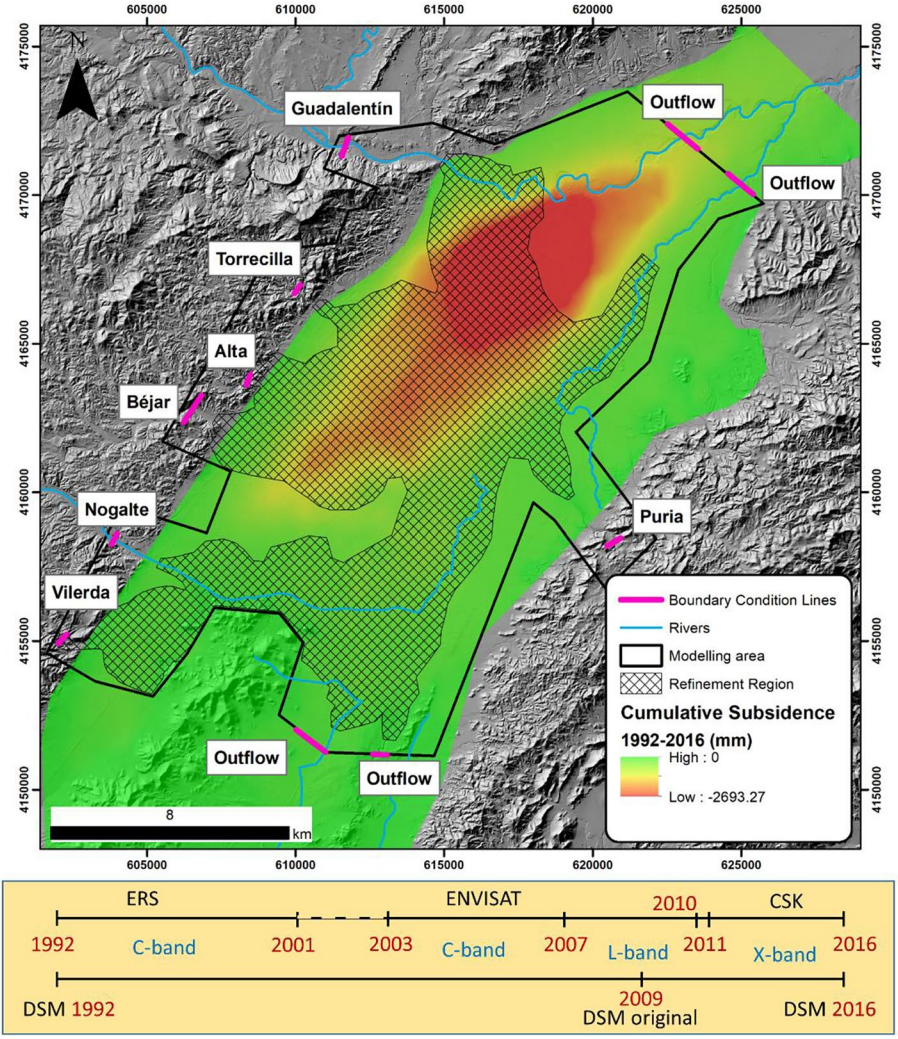

Fig. 3 Cumulative land subsidence after the integration of all InSAR data for the 1992–2016 period. The modelling area, mesh used for the refinement region and boundary inflow and outflow sections are also plotted in the map

software uses a hybrid approach that combines finite difference and finite volume methods based on the principles of mass conservation and momentum conservation (Cerri 2017; Shahverdi and Talebmorad 2023).

The 2D flow simulation algorithm of the HEC-RAS model involves two sets of equations to describe the motion of water throughout the computational mesh. The first set corresponds to the shallow water (SW) equations, also known as bidimensional Saint Venant equations (Brunner 2016). Notably, this equation assumes that the flow is incompressible and corresponds to the unsteady differential structure of mass conservation.

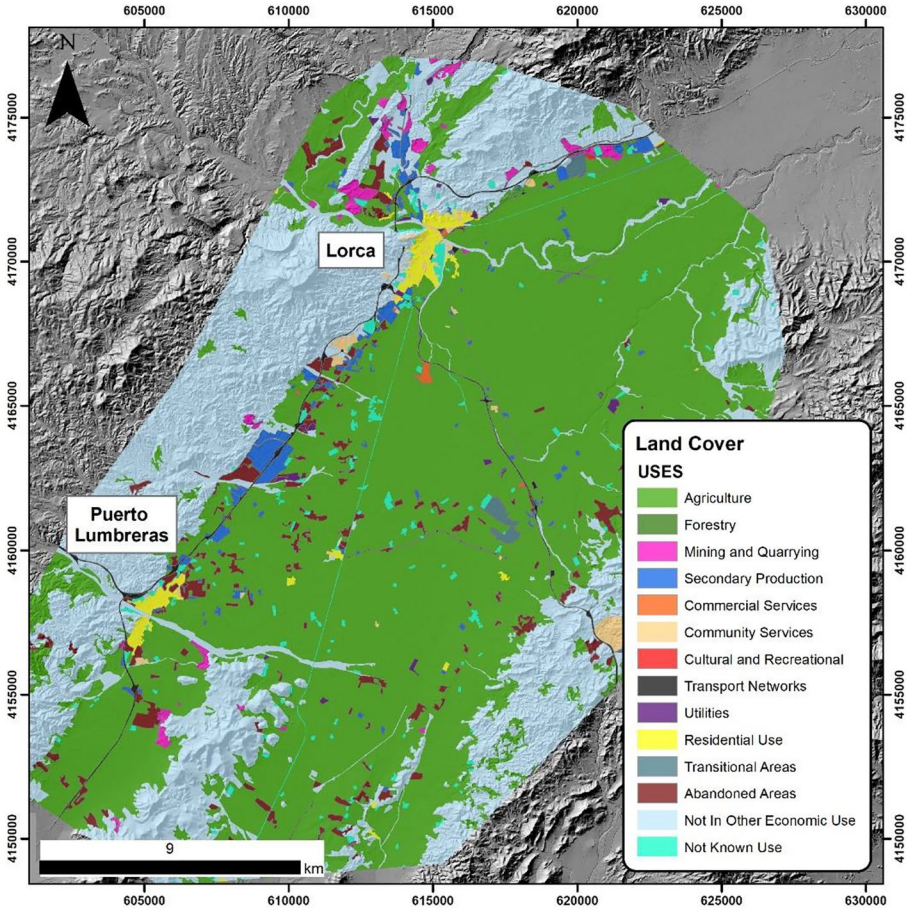

Fig. 4 Land cover map for the Alto Guadalentín valley

Regarding the second set of equations, the momentum conservation concept is applied in those cases where the horizontal scale greatly exceeds the vertical length scale, which suggests that the vertical velocity is low. In this situation, gravity and bottom friction are the dominant terms, and a new version of the shallow water equation, called the 2D diffusion wave momentum equation, can be obtained, whereby the vertical velocity and vertical derivative terms are ignored (Sarchani et al. 2020). For more information on the equations of HECRAS software, we refer the reader to the manual (Brunner 2016).

3.2.2 Geometry Data: 2D Flow Area

The first step before 2D hydraulic modelling is to validate the terrain model since the accuracy of the results strongly depends on the terrain data quality, as described in Section 3.1.3. The model area was discretized into square grid cells. A computational mesh with a grid size of 100 × 100 m was first used to discretize the 139 km^2 area (Fig. 3) into 1,423,334 cells, improving the computational time. The computational mesh was then

refined using subgrid units of 10 m × 10 m to improve the model results in certain areas (Fig. 3). The final limits of the computational mesh were defined through tentative pre-runs, avoiding unnecessary mesh refinement to reduce the total computational time for the definitive run.

3.2.3 Unsteady Flow Analysis

In unsteady flow analysis, the boundary conditions for each water course were determined based on flow hydrographs and energy slopes obtained from the DSM. The hydrographs were gradually increased over 6 h to maintain model stability and then maintained constant until the end of the simulation process (18 h). A default value of 1.0 was used for the weighting factor (theta) that determines the spatial derivatives. The tolerance for 2D water surface comparison was set to 0.91 m, with a maximum of 20 iterations. Hydraulic calculations were conducted at computation intervals of 5 s, while the hydrograph output, mapping output, and detailed output calculation intervals were all set to 10 min.

The downstream boundary condition of the HEC-RAS model is the normal depth option for the four outflows shown in Fig. 4. These input and output flow boundary conditions were kept constant under both temporal scenarios. To address the existing uncertainties related to the definition of the boundary conditions and their impacts on the results for the study area, the location of these lines was set sufficiently far (upwards and downwards) from the main study area.

3.3 Hazard and Risk Evaluation

3.3.1 Flood Hazard Estimation

The water velocity and water depth are two of the flood modelling variables provided by HEC-RAS software. With the use of this output information, the hazard risk in the Alto Guadalentín valley can be calculated. In this case, the methodology developed by the Ebro Basin Water Management Authority (CHS 2020) was applied. This methodology is an adaptation of the approach developed by the Department for Environment, Food and Rural Affairs of the United Kingdom, but the particular issues of the Spanish basins were considered through Eq. (1) (CHS 2020).

$$HR = d.(v + 0.5) + DF \tag{1}$$

where HR is the hazard risk index, d is the water depth, v is the velocity and DF is the debris flow coefficient. The value of the debris flow coefficient varies between 0 and 1, which depends on the water depth and land use, as shown in Table S2. Once the debris flow value is defined, the flood hazard risk can be calculated using Eq. (1), and the risk in the flooded areas can be classified by the HR value, as shown in Table S3.

3.3.2 Material Damage Cost Estimation

The methodology developed by the Spanish Ministry of Agriculture, Food and Environment was applied to economically evaluate the flood risk. In this approach, it is necessary to assign a monetary value to the flooded areas of various land uses and then apply a coefficient according to the water depth obtained via flood simulation (Eq. 2. (CHS 2020)).

$$Monetary\ value(€) = Flooded\ surface\left(m^2\right) \times unit\ value\left(\frac{€}{m^2}\right) \times hazard\ coefficient \tag{2}$$

In this classification, the hazard coefficient depends on the water depth (Table S4). In this approach, a value of 0.7 m was considered an inflection point. Above this value, which is the mean height for tables and counters, total damage occurs. Regarding the unit value, these costs were standardized by the land use value, as shown in Table S5.

4 Results

In this section, the hydraulic model results for the 1992 and 2016 scenarios are described. Under both scenarios, the layers of the maximum water depth, velocity and flood extent were extracted by means of RasMapper and processed in GIS software. Starting from this information, flood hazard and material cost estimations were conducted by combining the output model information with land cover use data and cadastral data based on the methodology detailed in Sections 3.2 and 3.3.

4.1 Flood Modelling Results

Figure 5a, b show the numerical model results for the two analysed scenarios (1992 and 2016). The 1992 scenario is characterized by water velocities varying between 0.02 and 14.34 m/s and water depths varying between 0.03 and 5.18 m (10th and 98th percentiles, respectively), with a total flooded area of 101.36 km^2. Accordingly, a water depth less than 0.3 m was registered in an area totalling 55.75 km^2, 24.42 km^2 exhibited a water depth of 0.3–0.7 m, 15.41 km^2 exhibited a water depth of 0.7–2.0 m and 5.78 km^2 exhibited a water depth of > 2.0 m (Tables S4 and 1). At the same time, the 2016 model is characterized by water velocities varying between 0.02 and 14.97 m/s and water depths varying between 0.02 and 5.06 m (10th and 98th percentiles, respectively), with a total flooded area of 103.4 km^2. Among them, 55.67 km^2 registered a water depth less than 0.3 m, 23.31 km^2 indicated a water depth of 0.3–0.7 m, 16.75 km^2 indicated a water depth of 0.7–2.0 m and 7.66 km^2 indicated a water depth of > 2.0 m.

4.1.1 Water Depth

Water depth maps for both scenarios are shown in Fig. 5a, b. In general, the most affected areas are not directly related to the most important waterflow course in the area (i.e., the Guadalentín River). In contrast, they are related to secondary stream courses such as the Torrecilla, Bejar and Nogalte ravines. Their entrance into the basin is represented by an alluvial fan structure with poorly developed channels except for the apical zone. This generates a large flood area with a low water depth slowly draining towards NE, searching for the exit of the valley.

Figure 5 shows the aerial extent of water depth threshold values of 0.3, 0.7 and 2.0 m, illustrating where possible damage could occur under both scenarios. These maps allow us to better analyse the consequences, in terms of potential flood damage, of the cumulative subsidence in the valley over the past decades. As shown in Fig. 5, the inundated area corresponding to values greater than 0.7 m has increased, coinciding with the area in which the highest rates of cumulative subsidence occur. With the input flow hydrographs

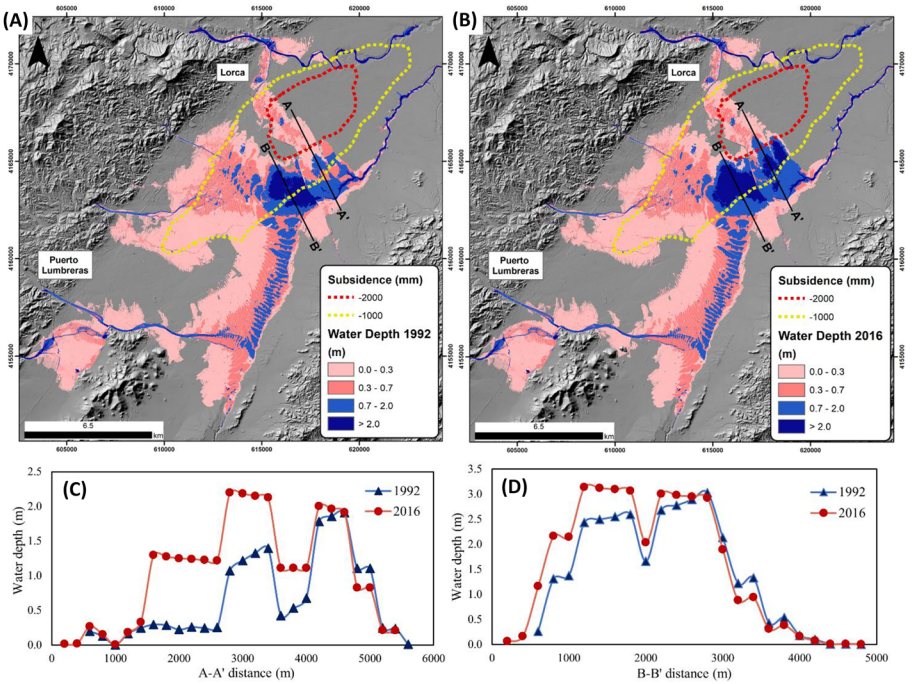

Fig. 5 **A** Water depth map for the 1992 and **B** 2016 scenarios. Note that the subsidence contours overlap. **C** and **D** Comparison between water depths in 1992 and 2016 along cross sections A-A' and B-B'

referring to a return period of 100 years, the water depth reaches more than 2 m in both cases corresponding with the main river channels. However, considering the subsidence progression effect, changes in the flood behaviour are detected, as summarized in Table 1. The total inundated area in 1992 was nearly 101.36 km^2, and in 2016, it was approximately 103.4 km^2. This represents an increase of 2.06% of the total flooded area (regardless of the water depth value). However, there were much larger relative differences when

Table 1 Water depth and velocity result comparison between the 1992 and 2016 scenarios

	Flooded area (km^2)		
Water depth (m)	**1992**	**2016**	**Difference**
0.0–0.3	55.75	55.67	-0.07
0.3–0.7	24.42	23.31	-1.11
0.7–2.0	15.41	16.75	1.34
> 2.0	5.78	7.66	1.87
Velocity range (m/s)	**1992**	**2016**	**Difference**
0.0–0.5	73.27	75.09	1.82
0.5–1.0	16.12	16.50	0.38
1.0–2.0	6.67	6.55	-0.13
2.0–5.0	4.78	4.74	-0.04
> 5.0	0.52	0.52	0.01

analysing high and low water depths: the flooded area with a water depth greater than 0.7 m increased by 15,21%. Moreover, the flooded area with a water depth less than 0.7 m decreased by 1.47%.

To analyse the water depth increase area, cross sections A-A' and B-B' displayed in Fig. 5 were installed across the valley along the NW−SE direction. As shown in Fig. 7a, b, the areas with greater changes could be identified. With the use of a sample range of 200 m, the water depth under the 1992 and 2016 scenarios was extracted to detect changes in the flooded area. The comparison results are shown in Fig. 5c, d, revealing that more remarkable changes occurred along cross-section A-A', showing that this area suffered an increase in the water depth near 1.5 m along the NW direction, while at the NE border, a decrease close to 0.5 m occurred. The main reason is the fact that the fastest subsidence area is located in the northwest centre of the basin, and this ground surface change induces flood spot migration towards this direction. A similar situation was observed in the B-B' cross section, in which the water depth increase reached approximately 0.8 m along the NW direction, decreasing close to 0.4 m along the SE direction. It could be concluded that the highest flood risk areas are increasing towards the highest subsidence area, reducing the flooding risk outside the subsidence bowl (SE limits of the valley).

The observed changes in the water flow maps between the two analysed scenarios do not affect the urban settlements located along the perimeter of the valley, but the rural population is spread across the centre of the valley. Urban settlements, such as Lorca city or Puerto Lumbreras, are located at higher elevations where the thinner, soft layers are less prone to intense subsidence.

4.1.2 Velocity

Water velocity maps are displayed in Fig. 6, in which there are changes in the flood extent under the 2016 scenario. Variations in flood behaviour patterns are located at the centre of the valley, coinciding with the subsidence areas. As expected, the zones with the highest velocities correspond to the river course, particularly the segments in the vicinity of

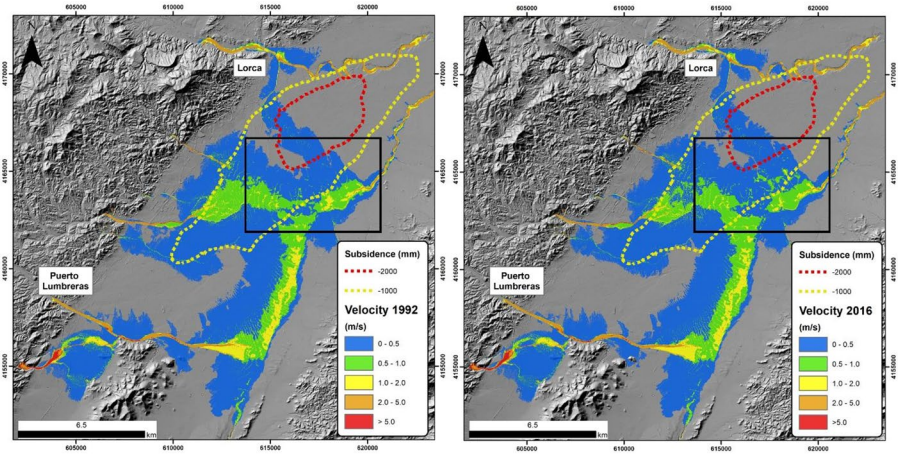

Fig. 6 Water flow velocity map for the 1992 and 2016 scenarios. The black squares denote the flooded area with changes. Note that subsidence contours are overlaid

the mountains where the slope is higher and near the mainstream courses where there are narrow channels and water flow has not yet surpassed its limits, such as the Vilerda ravine. Notably, the water flow presents a low velocity over very extended areas. This fact, which is common in flooded plain areas such as the Alto Guadalentin valley, also highlights the low drainage capacity in the area, producing long residence times. This undesirable characteristic worsens under the 2016 scenario at the confluence of the Nogalte and Torrecilla-Bejar waterflows, where the area with a 0–0.5 m/s velocity increased because of subsidence. This phenomenon is shown in Fig. 6 and more explicitly in Fig. 7b, where the difference in velocity between both scenarios is depicted.

Significant differences are found within the different velocity ranges (Table 1), which supports the change patterns highlighted by black squares in Fig. 6. These estimations reveal that from 1992 to 2016, the areas with velocities between 0.0 and 0.5 m/s increased by 2.5%, and the areas with velocities between 0.5 and 1.0 m/s increased by 2.4%. Concerning the decrease in the velocity value at the centre of the black square in 2016 relative to 1992, the flow dynamics were reduced or decelerated. This could be explained by the fact that this area matches the starting point of the highest subsidence domain boundary, which extends along the northwest direction and advances towards the centre of the valley, as shown in Fig. 3. Therefore, the water flow velocity diminishes at this point because the flood area is expanding towards the northwest due to the corresponding slope change.

Figure 7a, b show the spatial distribution of the differences in the water depth and velocity between 1992 and 2016. As shown in both layers, the greatest discrepancies are concentrated at the centre of the valley due to the proximity to areas with the highest cumulative subsidence that exhibit water depth differences ranging from 1–2 m and water velocity differences greater than 0.35 m/s. The maximum differences in the water depth, up to 2 m, agree with the maximum differences between both analysed scenarios, up to 2.5 m (Fig. 3). The most affected zone is mainly occupied by agricultural activities and farms. Urban areas and surrounding zones reveal minor changes, since most of them mainly occur near the mountains, where there is no subsidence. Therefore, the patterns of the rivers and ravines remain similar to the 1992 ground conditions.

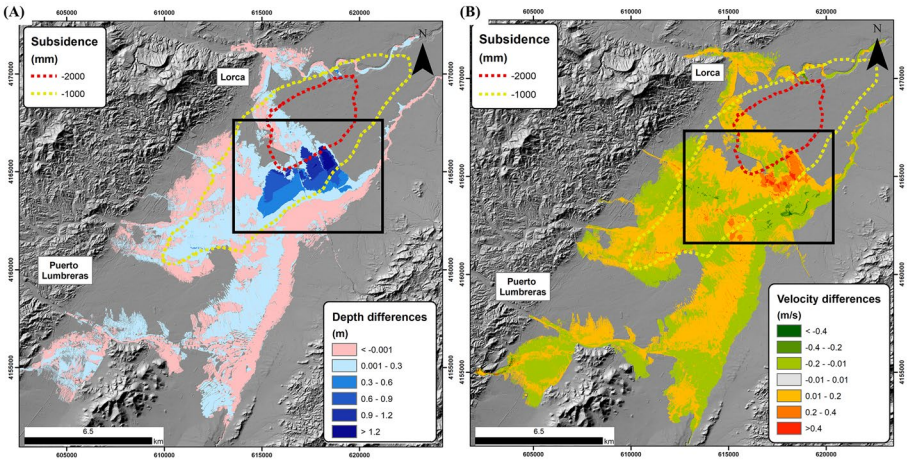

Fig. 7 Differences in the **A** water depth and **B** velocity between the 1992 and 2016 scenarios. The black squares denote the flooded area with changes. Note that subsidence contours are overlaid

4.2 Flood Hazard Classification and Economic Damage Estimation

Hazard risk maps for both scenarios are shown in Fig. 8a, b. The values are categorized into four hazard areas, namely, low, moderate, high and extreme, according to the classification described in Table S3. With the use of the water depth and velocity layers from the modelling outputs as input information in Eq. (1), hazard risk maps are obtained and reclassified to analyse the differences between 1992 and 2016. As previously mentioned, the area with the most important changes between the two scenarios is at the NW centre of the valley, matching the area affected by land subsidence. Notably, the water flows from the eastern part of the valley converge in this area. Figure 8a, b reveal that there is an increase in the hazardous areas, highlighted within the black square. The calculated differences in the hazard risk areas between both scenarios listed in Table 2 confirm that the moderate-risk areas increased by + 5.04%, the high-risk areas increased by + 30.17%, and the extreme-risk areas increased by + 5.62% relative to 1992 conditions.

Cross analysis of the hazard risk maps for 1992 and 2016 and the cadastral information obtained from the Spanish Cadastral website allowed us to perform a building-affected survey (Fig. 8c, d). In this analysis, the cadastral units for both urban and rural construction were employed. The buildings within the potential flood risk area under both scenarios

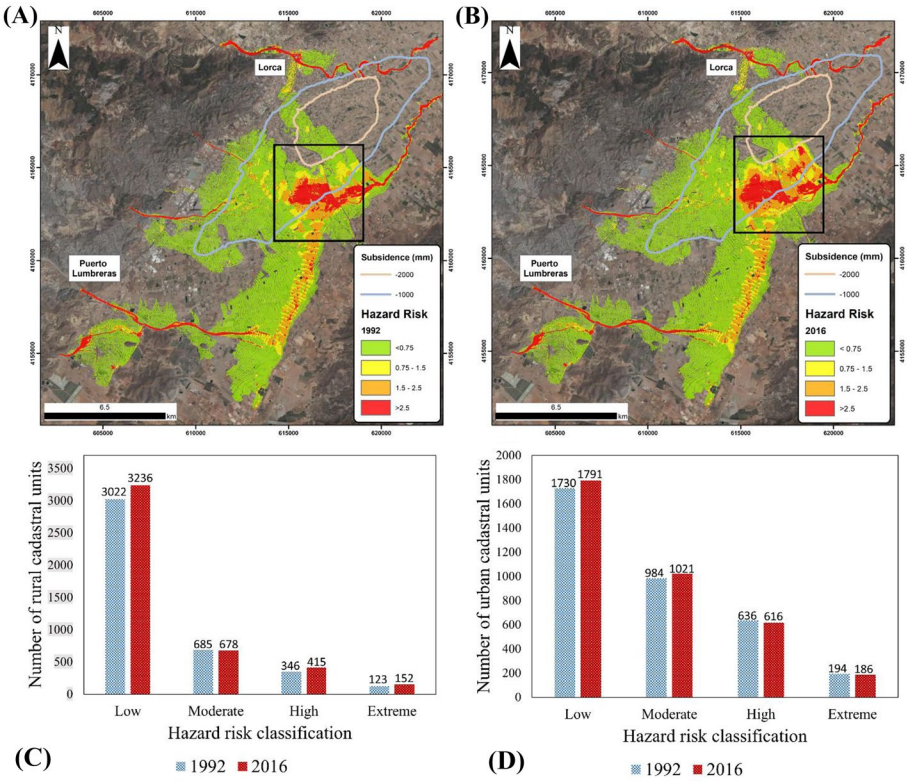

Fig. 8 **A** Hazard risk map for the 1992 and **B** 2016 scenarios. The black squares denote the flooded area with changes. Note that subsidence contours are overlaid. **C** and **D** Number of rural and urban buildings affected by different flood hazard risks under the 1992 and 2016 scenarios

Table 2 Monetary value results for each economic activity under the 1992 and 2016 scenarios

Classification	Hazard risk area (km^2)			
	1992	**2016**	**Difference**	%
Low	74.63	73.13	-1.50	-2.01
Moderate	8.95	9.40	+0.45	5.04
High	7.92	10.31	+2.39	30.17
Extreme	9.40	9.93	+0.53	5.62

were counted by discretizing them according to the hazard risk classification established in Table S3. Considering the results in Fig. 8c, d, the rural cadastral area shows the main increases in the number of units affected by the changes in the flood patterns induced by land subsidence, with an increase of 7.08% in the number of buildings at a low hazard risk, 19.94% at a high risk and 23.57% at an extreme risk. Moreover, the urban cadastral units at a low risk show an increase of only 3.53%, with an increase of 3.76% in urban cadastral units at a moderate risk. These differences can be explained by the fact that the main inundation area occurs at the centre of the valley occupied by rural construction and not in the cities, which are close to the mountains where subsidence is absent.

Finally, monetary value analysis was conducted to determine whether the progression of land subsidence over time may increase economic losses by increasing flash flooding hazards in the Alto Guadalentín valley. In this analysis, the methodology proposed by the Spanish Ministry of Agriculture Food and Environment was applied combined with the land cover use information established in the SIOSE (Fig. 4). In this land use classification, some polygons comprise more than one land use. As a consequence, these polygons may yield a different monetary value because of cost assignment according to the unit value items listed in Table S5 and discretization of SIOSE polygons based on the different economic activity classes contained in each geometry.

The monetary value calculation results are summarized in Table 3. At first glance, there is an increase in the economic loss of € 70,172,620 in the whole study area, which is additional evidence supporting the fact that subsidence may play a negative role in flooding behaviour modification. Furthermore, as mentioned before, floods mainly affect the agricultural area, which is the economic activity most impacted by changes in inundation patterns. The estimated difference in the economic impact within the agricultural area between the 1992 and 2016 scenarios is an increase of € 63,551,736. This value accounts for 90% of the total cost difference between the two analysed periods. This is primarily due to the dominance of agricultural activities in the valley, with these areas mainly concentrated at the centre of the basin where subsidence is higher, resulting in a significant impact on the spatial patterns of flooding. The second most important economic activity affected by flooding is transport networks, with an increase of € 9,473,857. This damage is mainly concentrated along the Lorca-Águilas highway, which crosses the critical flooding area and even produces a water dam effect. The drainage systems are not effective, and therefore, water may flow over the crest of embankments, producing notable erosion affecting the road. This important communication route was already affected by one of the last flood events in 2012 when a bridge collapsed after the failure of its foundations because of the local scour phenomenon. Commercial and community services also exhibit a slight increase. This can be attributed to the fact that these services are primarily concentrated in urban areas, which are situated closer to the mountains and farther away from the subsidence area, as well as the higher-flood risk zone.

Table 3 Monetary value results for each economic activity for the 1992 and 2016 scenarios

Land cover uses	1992 scenario		2016 scenario		Monetary value differences
	Area (km^2)	Monetary value	Area (km^2)	Monetary value	
Agriculture	88.27	871,903,146 €	90.40	935,454,882 €	63,551,736 €
Mining and quarrying	0.39	118,181 €	0.39	118,213 €	31 €
Secondary production	0.97	99,748,672 €	0.97	99,803,623 €	54,952 €
Commercial services	0.14	19,770,815 €	0.18	21,753,205 €	1,982,390 €
Community services	0.41	7,636,208 €	0.44	8,265,619 €	629,412 €
Transport networks	1.03	105,502,827 €	1.03	114,976,684 €	9,473,857 €
Utilities	0.30	81,978,897 €	0.31	81,278,805 €	-700,092 €
Residential uses	1.28	105,099,035 €	1.24	100,449,936 €	-4,649,099 €
Natural grassland	2.72	2,097,814 €	5.41	1,927,248 €	-170,566 €
Total	95.50	1,293,855,594 €	100.35	1,364,028,214 €	70,172,620 €

5 Discussion

As briefly mentioned in the Introduction, we considered the advantages of 2D models over 1D models, especially due to the geomorphological characteristics of the study area. Land subsidence owing to groundwater overexploitation mainly occurs in detrital aquifers, which are normally located in valleys or flat areas. While 1D models are suitable for areas where well-defined channels and a predominant longitudinal flow direction exist, they are not suitable for the Alto Guadalentin valley, where the main watercourses almost disappear when they enter into the valley and water flows of different directions occupy an extended area. As a result, the water velocity vector comprises two significant components along the two horizontal direction relative to the vertical direction. Therefore, the morphological features of the study area played a crucial role in the decision to employ 2D modelling over other approaches.

Land subsidence due to groundwater depletion is a slow and gradual process that develops on large time scales (months to years), which, even if it is not as fast as flooding, can produce significant long-term economic impacts on infrastructures and buildings. In this study, we demonstrated how when both phenomena are concomitant and affect the same area, the flood risk can be modified or even exacerbated in some areas. We addressed the changes in inundation patterns induced by land subsidence by modelling a 100-year return period flood event in the Alto Guadalentín valley. The effect of land subsidence on hydraulic modelling was considered by incorporating the cumulative lowering of the ground surface measured by InSAR in digital surface models. Hydraulic modelling revealed a significant increase in the maximum flood depth and the flooded inundation area in 2016 over 1992 levels (Fig. 7a, b).

Changes in the spatial distribution of flood propagation are also supported by the water velocity map combined with the cross-sectional profiles displayed in Fig. 5c, d, suggesting that land subsidence changes the spatial patterns of the flooding risk. The results show a migration of the inundation area towards the NW direction, where the maximum cumulative land subsidence (over 2.5 m in some zones) is responsible for an increase in the water depth and water velocity. The drainage capacity of the valley is another flood-related variable that is affected by subsidence in this case since the velocity rates show a decrease when

comparing both scenarios; this fact may lead to longer retention periods of accumulated water, which is another key factor in evaluating the flood economic impact.

The results also show a considerable increase in the risk classes, with an increase of 23.57% in the moderate-risk class, resulting from the migration of the inundation area to the most valuable areas. The combination of flood hazard maps and the cadastral unit layer also enabled the identification of significant increments in the hazard for rural units, with an increase of 29 buildings at an extreme risk and 99 buildings at a high risk under 2016 ground conditions. In absolute terms, the 2016 scenario revealed that approximately 152 rural cadastral units are at an extreme flood risk and 415 are at a high risk (Fig. 8c, d). These results agree with the reported damage due to the flooding in 2012, when more than 300 rural buildings, according to the Lorca municipally, and more than 353 buildings, according to the Puerto Lumbreras city council, were damaged. Discrepancies between the estimations and the recorded damage data principally occur because in 2012, the Nogalte ravine recorded nearly 2,000 m^3/s of runoff during an extraordinary rain event (García-tornel 2016), while in the performed simulations, a 100-year return period input flow data with a value of 487 m^3/s was used. Additionally, the economic damage caused by the extreme flood event in 2012 to sanitation structures, transport network and railway track from Lorca to Águilas in the Almendros was calculated at approximately € 159,900,000 (Gil-Meseguer et al. 2012), while the 2016 simulation revealed an economic cost of approximately € 196,075,489 for utilities and transport networks (Table 3). The flood, velocity and hazard risk maps developed in this study are of paramount importance for local authorities since a) they enable the identification of high-risk flooding zones in Alto Guadalentín Valley considering the effect of land subsidence; b) they can be used for the formulation of efficient management strategies and hazard and monetary cost evaluation for extreme flash floods; c) they provide relevant information for the design of a drainage plan for the highway; d) the results provide strategies to define the most affected areas not only at present but also considering the potential future movement of the flood risk in the case that the subsidence process continues. Even though the determined differences in the economic impact of a specific flood event because of the subsidence phenomenon are important, the economic impact could be much higher in other areas where land uses on both sides of the flooded area differ. In the Alto Guadalentín valley, the movement of the flood-affected area is relatively consistent, with agriculture as the main land use on both sides of the affected area.

6 Conclusion

In this study, two 2D HEC-RAS hydraulic models were established considering two terrain scenarios corresponding to 1992 and 2016 for the Alto Guadalentín valley (SE Spain). Both scenarios were obtained by considering the cumulative land subsidence registered by InSAR in the study area between these two times. It is important to highlight that the geomorphologic features were considered to decide the modelling approach; as such, it could be concluded that 2D models are preferred over 1D models due to the occurrence of land subsidence in detrital aquifers in flat areas. While 1D models are suitable for well-defined channels with predominant longitudinal flow, they are unsuitable for the ephemeral rivers and multidirectional water flows in the Alto Guadalentin valley during flash floods.

The first conclusion of this study reveals that subsidence must always be considered when evaluating the flood risk in affected areas. Notably, the impact of this phenomenon

depends on the geologic conditions of the study area and the magnitude of land subsidence. The case of the Alto Guadalentin valley, with cumulative land subsidence values up to 2.7 m over 14 years, is a prime example that illustrates this combined effect in inland basins. Moreover, the impact would increase if land subsidence occurred since the beginning of overexploitation in the 1960s.

Land subsidence phenomena alter the morphology of basins, creating new flood-affected areas and removing existing ones, and they also affect the maximum water depth and velocity during a flooding event. In this study, we showed that the flooding area modelled with a return period of 100 years increases up to 2.04 km^2. More importantly, the areas with a water depth greater than 0.7 m increased by 15.21% between 1992 and 2016. Changes in the flood patterns showed that the inundation area is expanding and migrating towards the NW direction, which agrees with the spatial distribution of land subsidence.

The velocity is also a hydraulic variable affected by the land subsidence process. The lowering of the ground surface creates more depressed areas, reducing the flow velocity, worsening the natural drainage conditions, and increasing the time during which lowlands are inundated. In inland and coastal areas affected by land subsidence, the drainage capacity can be reduced, and the economic impact of a potential flood event can increase.

Flood risk managers must consider the potential risk of subsidence when evaluating the flood risk and designing strategies and protection measures to ensure a more resilient society. The potential future movement of the flooded area as a consequence of the gradual lowering of the ground surface may negate ineffective strategies designed without considering land subsidence. The generated hazard maps provide useful information for the identification of areas prone to flooding and even enable the evaluation of future scenarios of flooding in land subsidence areas.

The results highlight the power of InSAR techniques for monitoring natural–anthropogenic phenomena and their applicability in flood hazard estimation management combined with high-resolution DSMs, land cover maps and cadastral information.

Supplementary Information The online version contains supplementary material available at https://doi.org/10.1007/s11269-023-03561-6.

Author Contributions **María I. Navarro-Hernández**: Conceptualization, Methodology, Modelling, Writing – original draft, Writing – re- view & editing, Supervision **Javier Valdés-Abellán**: Conceptualization, Methodology, Modelling, Writing – re- view & editing, Supervision. **Roberto Tomás**: Conceptualization, Methodology, Writing – review & editing, Supervision, Funding acquisition. **Serena Tessitore**: Conceptualization, Writing – review & editing, Supervision, **Pablo Ezquerro**: InSAR processing, Writing – review & editing, Supervision. **Gerardo Herrera**: Writing – review & editing, Supervision.

Funding Open Access funding provided thanks to the CRUE-CSIC agreement with Springer Nature. For this paper María Navarro-Hernandez is funded by the PRIMA programme supported by the European Union under grant agreement No 1924, project RESERVOIR. This research also was carried out in the framework of ESA-MOST China DRAGON-5 project (ref. 59339).

Data Availability The data that support the findings of this study are available in "Sede electronica del Catastro/Catastral electronic site" at www.sedecatastro.gob.es. These data were derived from the following resources available in the public domain: www.sedecatastro.gob.es.

Declarations

Ethical Approval All work is compliance with Ethical Standards.

Consent to Participate Authors give their permission.

Consent to Publish The authors give their permission.

Competing Interest The authors declare no conflict of interest. The funders had no role in the design of the study; in the collection, analyses, or interpretation of data; in the writing of the manuscript, or in the decision to publish the results.

References

Bartier PM, Keller CP (1996) Multivariate interpolation to incorporate thematic surface data using inverse distance weighting (IDW). Comput Geosci 22(7):795–799. https://doi.org/10.1016/0098-3004(96)00021-0

Bodoque JM, Amérigo M, Díez-Herrero A, García JA, Cortés B, Ballesteros-Cánovas JA, Olcina J (2016) Improvement of resilience of urban areas by integrating social perception in flash-flood risk management. J Hydrol 541:665–676. https://doi.org/10.1016/j.jhydrol.2016.02.005

Bonì R, Herrera G, Meisina C, Notti D, Béjar-Pizarro M, Zucca F, González PJ, Palano M, Tomás R, Fernández J, Fernández-Merodo JA, Mulas J, Aragón R, Guardiola-Albert C, Mora O (2015) Twenty-year advanced DInSAR analysis of severe land subsidence: The Alto Guadalentín Basin (Spain) case study. Eng Geol 198:40–52. https://doi.org/10.1016/j.enggeo.2015.08.014

Brunner GW (2016) HEC-RAS river analysis system hydraulic reference manual version 5.0. Hydrol Eng Cent 547

Calvo García-Tornel F (2016) Riego por avenida en laderas subáridas: el rio Guadalentín en Lorca. In Libro Homenaje al Profesor Alfredo Morales Gil (pp. 1049–1069). Servicio de Publicaciones de la UA. https://doi.org/10.14198/LibroHomenajeAlfredoMorales2016-47

Castejón Porcel G, Romero Díaz MA (2014) Inundaciones en la Región de Murcia en los inicios del siglo XXI. Biblio 3W Revista Bibliográfica de Geografía y Ciencias Sociales XIX(19):40–46. https://revistes.ub.edu/index.php/b3w/article/view/26085

Cerón JC (1995) Estudio Hidrogeoquímico del Acuífero del Alto Guadalentín. Universidad de Granada

Cerri M (2017) Flood simulation using HEC-RAS model calibrated with remotely sensed water mask: a case study of Mulde River. Technical University of Munich, Germany

CHS (2014) Sistema Nacional de Cartografía de Zonas Inundables: Demarcacion Hidrográfica del Segura, Mapas de Peligrosidad y Riesgo de Inundación

CHS (2020) Revisión y Actualización de los Mapas de Peligrosidad y Riesgo por Inundación de las Áreas con Riesgo Potencial Significativo de Inundación 2o Ciclo

Ezquerro P, Tomás R, Béjar-Pizarro M, Fernández-Merodo JA, Guardiola-Albert C, Staller A, Sánchez-Sobrino JA, Herrera G (2020) Improving multi-technique monitoring using Sentinel-1 and Cosmo-SkyMed data and upgrading groundwater model capabilities. Sci Total Environ 703:134757. https://doi.org/10.1016/j.scitotenv.2019.134757

Fernandez J, Prieto JF, Escayo J, Camacho AG, Luzón F, Tiampo KF, Palano M, Abajo T, Pérez E, Velasco J, Herrero T, Bru G, Molina I, López J, Rodríguez-Velasco G, Gómez I, Mallorquí JJ (2018) Modeling the two- and three-dimensional displacement field in Lorca, Spain, subsidence and the global implications. Sci Rep 8(1):1–15. https://doi.org/10.1038/s41598-018-33128-0

Ferretti A, Monti-Guarinieri A, Prati C, Rocca F (2007) InSAR principles: Guidelines for SAR interferometry processing and interpretation. ESA Publications

Gil-Meseguer E, Pérez-Morales A, Gómez-Espín J (2012) Precipitaciones y avenidas del 28 de septiembre del 2012 en el cuadrante suroccidental de la cuenca del Segura, (Municipios de Lorca, Puerto Lumbreras y Pulpí). Papeles de Geografía 55(56):75–94

Herrera-García G, Ezquerro P, Tomas R, Béjar-Pizarro M, López-Vinielles J, Rossi M, Mateos RM, Carreón-Freyre D, Lambert J, Teatini P, Cabral-Cano E, Erkens G, Galloway D, Hung WC, Kakar N, Sneed M, Tosi L, Wang H, Ye S (2021) Mapping the global threat of land subsidence. Science 371(6524):34–36. https://doi.org/10.1126/science.abb8549

Hutanu E, Mihu-Pintilie A, Urzica A, Paveluc LE, Stoleriu CC, Grozavu A (2020) Using 1D HEC-RAS modeling and LiDAR data to improve flood hazard maps accuracy: A case study from Jijia Floodplain (NE Romania). Water (Switzerland) 12(6):1–21. https://doi.org/10.3390/w12061624

Lauchlan Arrowsmith CS, Zhu Y (2014) Comparison between 2D and 3D Hydraulic modelling approaches for simulation of vertical slot fishways. ISHS 2014 - Hydraulic Structures and Society - Engineering Challenges and Extremes: Proceedings of the 5th IAHR International Symposium on Hydraulic Structures, June, 25–27. https://doi.org/10.14264/uql.2014.49

Lea D, Yeonsu K, Hyunuk A (2019) Case study of HEC-RAS 1D–2D coupling simulation: 2002 Baeksan flood event in Korea. Water (Switzerland) 11(10):1–14. https://doi.org/10.3390/w11102048

Marchi L, Borga M, Preciso E, Gaume E (2010) Characterisation of selected extreme flash floods in Europe and implications for flood risk management. J Hydrol 394(1–2):118–133. https://doi.org/10.1016/j.jhydrol.2010.07.017

Mihu-Pintilie A, Cîmpianu I, Stoleriu CC, Paveluc LE (2019) Using high-density LiDAR data and 2D streamflow hydraulic modeling to improve urban flood hazard. Water 11(1832):1–24

Ministerio de Medio Ambiente, y M. R. y M (2011) Guía Metodológica para el desarrollo del Sistema Nacional de Cartografía de Zonas Inundables. https://www.miteco.gob.es/es/agua/publicaciones/guia_snczi_baja_optimizada_tcm30-422920.pdf

National Weather Service (2019) Natural hazard statistics. https://www.weather.gov/hazstat/. Accessed April 2022

Ortega-Becerril JA, Garzón G, Béjar-Pizarro M, JesúsMartínez-Díaz J (2016) Towards an increase of flash flood geomorphic effects due to gravel mining and ground subsidence in Nogalte stream (Murcia, SE Spain). Nat Hazard 16(10):2273–2286. https://doi.org/10.5194/nhess-16-2273-2016

Poreh D, Pirasteh S, Cabral-Cano E (2021) Assessing subsidence of Mexico City from InSAR and LandSat ETM+ with CGPS and SVM. Geoenviron Disasters 8:1. https://doi.org/10.1186/s40677-021-00179-x

Pujadas Ferrer J (2002) Las inundaciones en España: Impacto económico y gestión del riesgo. In Riesgos Naturales (pp. 879–888). Ariel

Refice A, D'Addabbo A, Capolongo D (2018) Flood monitoring through Remote Sensing. Springer

Romera-Franco J (2008) Vulnerabilidad y riesgo de inundación en el espacio urbano de Lorca: de la retrospectiva histórica a la situación actual. Ayuntamiento de Lorca. Archivo Municipal. Número 4–5

Sarchani S, Seiradakis K, Coulibaly P, Tsanis I (2020) Flood inundation mapping in an ungauged basin. Water (switzerland) 12(6):1–21. https://doi.org/10.3390/W12061532

Scarpino S, Albano R, Cantisani A, Mancusi L, Sole A, Milillo G (2018) Article multitemporal SAR data and 2D hydrodynamic model flood scenario dynamics assessment. ISPRS Int J Geo Inf 7(3):1–24. https://doi.org/10.3390/ijgi7030105

Schumann AH (2011) Flood risk assessment and management. In Flood Risk Assessment and Management: How to Specify Hydrological Loads, Their Consequences and Uncertainties. Springer. https://doi.org/10.1007/978-90-481-9917-4_11

Sempere CM, del Rosario Vidal-Abarca M, Suárez ML (1994) Floods in arid south-east Spanish areas: a historical and environmental review. In G. Rossi, N. Harmancioğlu, & V. Yevjevich (Eds.), Coping with Floods (Vol. 257, pp. 271–278). Springer Netherlands. https://doi.org/10.1007/978-94-011-1098-3_16

Şen Z (2017) Flood modeling, prediction and mitigation. Springer, In Flood Modeling, Prediction and Mitigation. https://doi.org/10.1007/978-3-319-52356-9

Shahverdi K, Talebmorad H (2023) Automating HEC-RAS and linking with particle swarm optimizer to calibrate manning's roughness coefficient. Water Resour Manag 37(2):975–993. https://doi.org/10.1007/s11269-022-03422-8

Smith K (2013) Enviromental hazards: Assesing risk and reducing disaster (Routledge, Ed.; Sixth, Issue 2). Taylor & Francis. https://doi.org/10.4324/9780203805305

Xu Y, Wang X, Jiang Z, Liu Y, Zhang L, Li Y (2023) An improved fineness flood risk analysis method based on digital terrain acquisition. Water Resour Manag. https://doi.org/10.1007/s11269-023-03535-8

Authors and Affiliations

María I. Navarro-Hernández[1] · Javier Valdes-Abellan[1] · Roberto Tomás[1] · Serena Tessitore[2] · Pablo Ezquerro[3] · Gerardo Herrera[3]

✉ María I. Navarro-Hernández
mainnahe@ua.es

Javier Valdes-Abellan
javier.valdes@ua.es

Roberto Tomás
roberto.tomas@ua.es

Serena Tessitore
s.tessitore@almaviva.it

Pablo Ezquerro
p.ezquerro@igme.es

Gerardo Herrera
g.herrera@igme.es

[1] Department of Civil Engineering, Escuela Politécnica Superior, University of Alicante, P.O. Box 99, Alicante 03080, Spain

[2] Almaviva Digitaltec, Centro Direzionale, Isola F8, Naples 80143, Italy

[3] Geohazards InSAR Laboratory and Modeling Group (InSARlab), Geoscience Research Department, Geological Survey of Spain (IGME), Alenza 1, Madrid 28003, Spain